Inorganic Chemistry

Article

pubs.acs.org/IC

Comproportionation Reactions to Manganese(III/IV) Pivalate Clusters: A New Half-Integer Spin Single-Molecule Magnet

Shreya Mukherjee,[†] Khalil A. Abboud,[†] Wolfgang Wernsdorfer,[‡] and George Christou*,[†]

[†]Department of Chemistry, University of Florida, Gainesville, Florida 32611-7200, United States

[‡]Institut Néel, CNRS/UJF, BP 166, 25 Avenue des Martyrs, 38042, Grenoble, Cedex 9, France

Supporting Information

ABSTRACT: The comproportionation reaction between Mn^{II} and Mn^{VII} reagents under acidic conditions has been investigated in the presence of pivalic acid as a route to new high oxidation state manganese pivalate clusters containing some Mn^{IV}. The reaction of $Mn(O_2CBu^t)_2$ and $NBu^n_4MnO_4$ with an excess of pivalic acid in the presence of $Mn(ClO_4)_2$ and NBu^n_4Cl in hot MeCN led to the isolation of $[Mn_8O_6(OH)(O_2CBu^t)_9Cl_3(Bu^tCO_2H)_{0.5}(MeCN)_{0.5}]$ (**1**). In contrast, the reaction of $Mn(NO_3)_2$ and $NBu^n_4MnO_4$ in hot MeCN with an excess of pivalic acid gave a different octanuclear complex, $[Mn_8O_9(O_2CBu^t)_{12}]$ (**2**). The latter reaction but with $Mn(O_2CBu^t)_2$ in place of $Mn(NO_3)_2$, and in a MeCN/THF solvent medium, gave $[Mn_9O_7(O_2CBu^t)_{13}(THF)_2]$ (**3**). Complexes **1**−**3** possess rare or unprecedented Mn_x topologies: **1** possesses a $[Mn^{III}_7Mn^{IV}(\mu_3\text{-}O)_4(\mu_4\text{-}O)_2(\mu_3\text{-}OH)(\mu_4\text{-}Cl)(\mu_2\text{-}Cl)]^{8+}$ core consisting of two body-fused Mn_4 butterfly units attached to the remaining Mn atoms via bridging O^{2-}, OH^-, and Cl^- ions. In contrast, **2** possesses a $[Mn_6^{IV}Mn_2^{III}(\mu_3\text{-}O)_6(\mu\text{-}O)_3]^{12+}$ core consisting of two $[Mn_3O_4]$ incomplete cubanes linked by their O^{2-} ions to two Mn^{III} atoms. The cores of **1** and **2** are unprecedented in Mn chemistry. The $[Mn^{III}_9(\mu_3\text{-}O)_7]^{13+}$ core of **3** also contains two body-fused Mn_4 butterfly units, but they are linked to the remaining Mn atoms in a different manner than in **1**. Solid-state direct current (dc) and/or alternating current (ac) magnetic susceptibility data established $S = {}^{15}/_2$, $S = 2$, and $S = 1$ ground states for **1**·MeCN, **2**·${}^1/_4$MeCN, and **3**, respectively. The ac susceptibility data also revealed nonzero, frequency-dependent out-of-phase (χ''_M) signals for **1**·MeCN at temperatures below 3 K, suggesting possible single-molecule magnet behavior, which was confirmed by single-crystal magnetization vs dc field scans that exhibited hysteresis loops. The combined work thus demonstrates the continuing potential of comproportionation reactions for isolating high oxidation state Mn_x clusters, and the sensitivity of the product identity to minor changes in the reaction conditions.

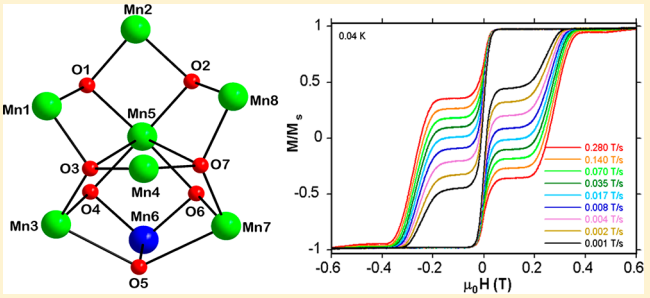

INTRODUCTION

Paramagnetic 3d metal clusters continue to attract a great deal of attention for a variety of reasons, such as their relevance to disparate areas such as bioinorganic chemistry and nanoscale magnetic materials. In Mn chemistry, one unifying theme between these areas is that both almost always involve the higher Mn oxidation states (Mn^{III}/Mn^{IV}), either wholly or in combination with the lower Mn^{II} state. In bioinorganic chemistry, the oxidizing power of the higher Mn oxidation states is at the heart of the evolution of Mn-containing redox enzymes, such as the oxygen-evolving complex (OEC), also known as the water-oxidizing complex (WOC), near photosystem II (PSII) of plants and cyanobacteria.[1,2] This is responsible for the sunlight-driven oxidation of water to oxygen gas, which is thermodynamically an extremely challenging transformation. The OEC is now known to comprise a $[Mn_3CaO_4]$ cubane unit to which is attached a fourth, external Mn ion. This oxidizing strength of Mn^{III} and Mn^{IV}, as well as the even stronger oxidant Mn^{VII}, also form the foundation of the long history of the use of Mn compounds as oxidizing agents for a large variety of organic compounds.[3,4] In the arena of nanoscale magnetic materials, Mn_x clusters containing Mn^{III} often possess a large ground state spin (S) because of the presence of ferromagnetic interactions and/or spin frustration effects,[5] and in combination with a sufficiently large easy-axis magnetic anisotropy (i.e., negative zero-field splitting parameter D), such clusters can be single-molecule magnets (SMMs).[6] These are molecules that function as nanoscale magnets below their blocking temperature (T_B),[6,7] and they also display interesting quantum properties such as quantum tunneling of the magnetization (QTM)6,[8] and quantum phase interference (QPI).[9] The presence of octahedral Mn^{III} is pivotal for making Mn SMMs, since Jahn−Teller elongated Mn^{III} has significant easy-axis anisotropy (negative D), in contrast to essentially isotropic Mn^{II} and Mn^{IV}.

There is thus a continuing interest in developing synthetic strategies to new Mn^{III}-containing SMMs of various metal

Received: September 17, 2012
Published: December 28, 2012

   dx.doi.org/10.1021/ic302021a | Inorg. Chem. 2013, 52, 873−884

Table 1. Crystallographic Data for 1·3MeCN, 2·MeCN, and $3\cdot{}^{1}/_{3}THF\cdot{}^{2}/_{3}MeCN$

parameter	1·3MeCN	2·MeCN	$3\cdot{}^{1}/_{3}THF\cdot{}^{2}/_{3}MeCN$
formula[a]	$C_{54.5}H_{97}N_{3.5}O_{26}Cl_3Mn_8$	$C_{60}H_{108}O_{33}Mn_8$	$C_{73}H_{133}Mn_9O_{35}$
fw,[a] g mol^{-1}	1763.23	1796.98	2065.25
crystal system	triclinic	monoclinic	orthorhombic
space group	$P\bar{1}$	$P2_1/n$	$Aba2$
a, Å	14.045(4)	15.010(2)	20.555(3)
b, Å	14.666(4)	21.876(4)	68.895(9)
c, Å	22.284(6)	26.275(4)	21.549(3)
α, deg	80.803(4)	90	90
β, deg	88.478(4)	98.750(8)	90
γ, deg	64.989(4)	90	90
V, Å^3	4101.8(19)	8527(2)	30516(7)
Z	2	4	12
T, °C	173(2)	173(2)	173(2)
radiation, Å[b]	0.71073	0.71073	0.71073
ρ_{calc}, mg/m^3	1.428	1.400	1.349
μ, mm^{-1}	1.355	1.219	1.150
$R1$[c,d]	0.0577	0.0369	0.0388
$wR2$[e]	0.1570	0.0947	0.0846

[a]Including solvate molecules. [b]Graphite monochromator. [c]$I > 2\sigma(I)$. [d]$R1 = [\sum||F_o| - |F_c||]/\sum|F_o|$. [e]$wR2 = [\sum[w(F_o^2 - F_c^2)^2]/\sum[w(F_o^2)^2]]^{1/2}$, $w = 1/[\sigma^2(F_o^2) + [(ap)^2 + bp]$, where $p = [\max(F_o^2, O) + 2F_c^2]/3$.

topologies, nuclearities, and ground state S values. In fact, it is also important to avoid the presence of Mn^{II} if possible, because Mn^{II} leads to weak exchange coupling and low-lying excited states, which are deleterious to good SMM behavior. Unfortunately, there are few commercially available Mn^{III} starting materials, and most Mn^{III}-containing SMMs and other clusters have been prepared from aerial oxidation of Mn^{II} under basic conditions, which often gives mixed Mn^{II}/Mn^{III} products. For this reason, we have in the past occasionally used a comproportionation approach to Mn^{III}-containing products, namely, the reaction of Mn^{II} with Mn^{VII} (MnO_4^-), such as for the preparation of $[Mn_4O_2(O_2CPh)_7(H_2O)_2]^-$[10] and $[Mn_4O_2(O_2CR)_7(pic)_2]^-$ salts (picH = piclinic acid), shown in eq 1.[11]

$$4Mn^{2+} + Mn^{7+} \rightarrow 5Mn^{3+} \quad (1)$$

The precedent for this approach in Mn^{III} carboxylate cluster chemistry was provided, of course, by the synthesis of $\{[Mn^{III}_3O(O_2CMe)_6](O_2CMe)(HO_2CMe)\}_n$ from the reaction of $Mn(O_2CMe)_2\cdot 4H_2O$ with $KMnO_4$ in acetic acid,[12] and Lis' synthesis of $[Mn^{III/IV}_{12}O_{12}(O_2CMe)_{16}(H_2O)_4]\cdot 2MeCO_2H\cdot 4H_2O$ from a lower Mn^{II}:Mn^{VII} ratio.[13] These also emphasize that control of the Mn^{II}:Mn^{VII} ratio can provide a convenient means to target mixed Mn^{III}/Mn^{IV} products, which can often help prevent complications from low-lying excited states compared with Mn^{II}/Mn^{III} and Mn^{III}/Mn^{III} couplings.[14] Indeed, it should be noted that the comproportionation reaction of Mn^{II} with Mn^{VII} to give Mn^{IV}−containing products has much more commonly been employed for the preparation of small nuclearity products with N-based chelating ligands such as 2,2′-bipyridine, 1,10-phenanthroline, and many others.[15]

In the present work, we have explored comproportionation reactions between Mn^{II} salts and Mn^{VII} in the presence of pivalic acid as a potential route to new Mn_x pivalate clusters. It was anticipated that the difference in bulk and the higher pK_a of pivalic acid (pK_a = 5.03) compared with acetic acid (pK_a = 4.75) and benzoic acid (pK_a = 4.20) would allow access to distinctly different manganese complexes.[16] We also employed a lower than normal Mn^{II}:Mn^{VII} ratio to target formation of Mn^{IV}-containing products. This work has successfully led to two Mn_8 and one Mn_9 pivalate products, with the former two being of unprecedented structural types. The syntheses, structures and magnetochemical characterizations of these complexes are described in this paper.

EXPERIMENTAL SECTION

Syntheses. All manipulations were performed under aerobic conditions using chemicals (reagent grade) and solvents as received. $NBu^n_4MnO_4$[17] and $Mn(O_2CBu^t)_2$[18] were prepared as previously reported.

Caution! *Perchlorate salts are potentially explosive; such compounds should be synthesized and used in small quantities, and treated with utmost care at all times.*

*$[Mn_8O_6(OH)(O_2CBu^t)_9Cl_3(Bu^tCO_2H)_{0.5}(MeCN)_{0.5}]$ (**1**).* To a stirred solution of $Mn(O_2CBu^t)_2\cdot 2H_2O$ (0.16 g, 0.50 mmol) and Bu^tCO_2H (2.83 mL, 24.6 mmol) in hot MeCN (20 mL, ∼80 °C) was added solid $Mn(ClO_4)_2\cdot 6H_2O$ (0.18 g, 0.50 mmol) and NBu^n_4Cl (0.14 g, 0.50 mmol). The light pink slurry was stirred for 5 min, and then solid $NBu^n_4MnO_4$ (0.18 g, 0.50 mmol) was slowly added in small portions, resulting in the formation of a dark brown-black solution. This was stirred for a further 15 min, allowed to cool to ambient temperature, filtered, and the filtrate was allowed to stand undisturbed at room temperature. After 2 weeks, the resulting X-ray quality dark brown crystals of **1**·3MeCN were collected by filtration and dried in vacuo. The yield was 25%. Anal. Calcd (Found) for **1**·MeCN ($C_{50.5}H_{91.5}N_{1.5}Mn_8O_{26}Cl_3$): C, 36.06 (35.77); H, 5.48 (5.33); N, 1.25 (1.31). Selected IR data (cm^{-1}): 3392 (w), 2971 (m), 2874 (s), 1671 (s), 1533 (s), 1484 (s), 1458 (m), 1421 (s), 1378 (s), 1364 (s), 1226 (s), 1032 (m), 938 (m), 896 (m), 656 (s), 621 (s), 597 (s), 480 (m), 458 (m).

*$[Mn_8O_9(O_2CBu^t)_{12}]$ (**2**).* To a stirred solution of $Mn(NO_3)_2$ (0.09 g, 0.50 mmol) and Bu^tCO_2H (1.89 mL, 16.4 mmol) in hot MeCN (25 mL, ∼80 °C) was slowly added $NBu^n_4MnO_4$ (0.27 g, 0.75 mmol). The solution was stirred for 15 min during which time the pink slurry changed to a dark red solution. The solution was allowed to cool to ambient temperature, filtered, and the filtrate allowed to stand undisturbed at room temperature. X-ray quality deep red crystals of **2**·MeCN slowly grew over a week, and they were collected by filtration and dried in vacuo. The yield was 36%. Anal. Calcd (Found) for $\mathbf{2}\cdot{}^{1}/_{4}MeCN$ ($C_{60.5}H_{108.75}N_{0.25}Mn_8O_{33}$): C, 40.21 (40.37); H, 6.07

dx.doi.org/10.1021/ic302021a | Inorg. Chem. 2013, 52, 873−884

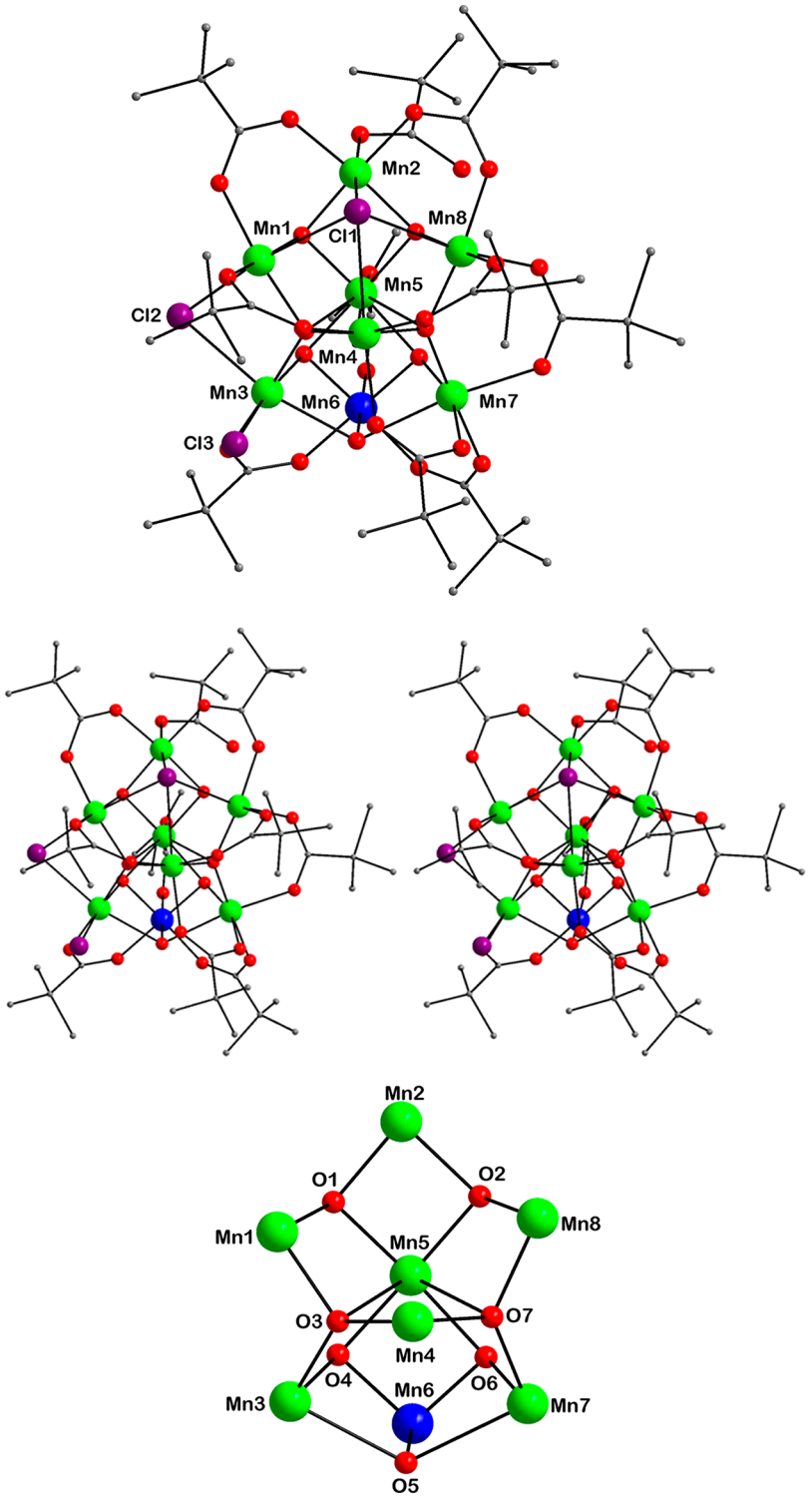

Figure 1. Structure of complex **1** (top), a stereopair (middle), and the labeled core (bottom). H atoms have been omitted for clarity. Color code: Mn^{IV} blue; Mn^{III} green; O red; Cl purple; C gray.

(6.14); N, 0.19 (0.21). Selected IR data (cm^{-1}): 3442 (w), 2965 (m), 2930 (m), 1599 (s), 1529 (m), 1482 (s), 1416 (s), 1362 (m), 1223 (s), 1031 (m), 937 (m), 893 (m), 785(m), 721 (m), 621 (s), 570 (m), 453 (m).

$[Mn_9O_7(O_2CBu^t)_{13}(THF)_2]$ ***(3)***. To a stirred solution of Mn-$(O_2CBu^t)_2{\cdot}2H_2O$ (0.16 g, 0.50 mmol) and Bu^tCO_2H (1.89 mL, 16.4 mmol) in hot MeCN/THF (20 mL, 2:1 v/v, ~80 °C) was slowly added solid $NBu^n_4MnO_4$ (0.18 g, 0.50 mmol) in small portions. The solution was stirred for 15 min during which time the pink slurry changed to a dark brown solution. This was allowed to cool to ambient temperature, filtered, and the filtrate allowed to stand undisturbed at room temperature. X-ray quality black crystals of $\mathbf{3}{\cdot}{}^1/_3THF{\cdot}{}^2/_3MeCN$ slowly grew over 3 days and were collected by filtration and dried in vacuo. The yield was 35%. Dried solid analyzed as solvent-free. Anal. Calcd (Found) for **3** ($C_{73}H_{133}Mn_9O_{35}$): C, 42.45 (42.81); H, 6.50 (6.90); N, 0.00 (0.00). Selected IR data (cm^{-1}): 2964 (m), 2928 (m), 1565 (s), 1484 (s), 1424 (s), 1375 (m), 1360 (m), 1228 (s), 1045 (m), 893 (m), 787 (m), 699 (m), 674 (m), 625 (s), 453 (m), 471 (m).

dx.doi.org/10.1021/ic302021a | *Inorg. Chem.* 2013, 52, 873−884

X-ray Crystallography. Data were collected on a Siemens SMART PLATFORM equipped with a CCD area detector and a graphite monochromator utilizing Mo K_α radiation (λ = 0.71073 Å). Suitable crystals of **1**·3MeCN, **2**·MeCN, and **3**·$^1/_3$THF·$^2/_3$MeCN were attached to glass fibers using silicone grease and transferred to a goniostat where they were cooled to 173 K for data collection. Data collection parameters are listed in Table 1. Cell parameters were refined using 8192 reflections. A full sphere of data (1850 frames) was collected using the ω-scan method (0.3° frame-width). The first 50 frames were remeasured at the end of data collection to monitor instrument and crystal stability (maximum correction on I was <1%). Absorption corrections by integration were applied based on measured indexed crystal faces. The structure was solved by the direct methods in SHELXTL6,[19] and refined on F^2 using full-matrix least-squares cycles. The non-H atoms were treated anisotropically, whereas the H atoms were placed in calculated, ideal positions and were refined as riding on their respective C atoms.

For **1**·3MeCN, the asymmetric unit consists of a Mn_8 cluster and two MeCN molecules in a general position, one of which is disordered. One of the pivalic acid ligands (O20) is disordered against a coordinated MeCN ligand (N3) and two partial MeCN molecules nearby in the lattice. The disordered atoms of the solvent molecules were constrained to remain equivalent during the refinement. Five of the coordinated pivalate ligands show the common rotational disorder of their Me groups, and these were refined in two sites each. 814 parameters were included in the final cycle of refinement using 10979 reflections with $I > 2\sigma(I)$ to yield R_1 and wR_2 of 5.77 and 15.70%, respectively.

For **2**·MeCN, the asymmetric unit consists of a Mn_8 cluster and a MeCN solvent molecule. The latter was too disordered to be modeled properly, thus program SQUEEZE,[20] a part of the PLATON package of crystallographic software, was used to calculate the solvent disorder area and remove its contribution to the overall intensity data. A total of 950 parameters were included in the final cycle of refinement using 15351 reflections with $I > 2\sigma(I)$ to yield R_1 and wR_2 of 3.69 and 9.47%, respectively.

For **3**·$^1/_3$THF·$^2/_3$MeCN, the asymmetric unit consists of a Mn_9 cluster in a general position, a half Mn_9 cluster located on a 2-fold rotation axis, a THF solvent molecule disordered around a 2-fold rotation axis, and an MeCN solvent molecule in a general position. The solvent molecules were again too disordered to be modeled properly, and SQUEEZE was used to remove their contribution to the overall intensity data. One pivalate ligand (C102) has the Me groups disordered because of symmetry, and each disordered atom was given a 0.5 occupancy. The cluster in a general position has five disordered pivalates (C11, C20, C39, C44, and C65), and each was refined in two parts with their site occupancies independently refined. A total of 1586 parameters were included in the final cycle of refinement using 28402 reflections with $I > 2\sigma(I)$ to yield R_1 and wR_2 of 3.88 and 8.46%, respectively.

Other Studies. Infrared spectra were recorded in the solid state (KBr pellets) on a Nicolet Nexus 670 FTIR spectrometer in the 400–4000 cm^{-1} range. Elemental analyses (C, H, and N) were performed by the in-house facilities of the University of Florida, Chemistry Department. Variable-temperature direct current (DC) and alternating current (AC) magnetic susceptibility data were collected on a Quantum Design MPMS-XL SQUID susceptometer equipped with a 7 T magnet and operating in the 1.8–300 K range. Pascal's constants[21] were used to estimate the diamagnetic corrections, which were subtracted from the experimental susceptibilities to give the molar paramagnetic susceptibilities (χ_M). Low temperature (<1.8 K) hysteresis studies were performed at Grenoble using an array of micro-SQUIDS.[22] The high sensitivity of this magnetometer allows the study of single crystals of SMMs of the order of 10–500 μm. The field can be applied in any direction by separately driving three orthogonal coils. Crystals were maintained in mother liquor to avoid degradation and were covered with grease for protection during transfer to the micro-SQUID and subsequent cooling.

RESULTS AND DISCUSSION

Syntheses. Many reaction systems were systematically explored, varying in Mn^{II}:Mn^{VII} ratio, additional reagents, and solvent ratio, in developing the procedures described here. The initial Mn^{II}:Mn^{VII} ratio employed was such as to give an average Mn oxidation state in the reaction of +4.5 or greater (eq 2).

$$Mn^{2+} + Mn^{7+} \rightarrow 2Mn^{4.5+} \quad (2)$$

This might seem higher than necessary, since we did not expect any Mn^V-containing products, but was designed to maximize the chances of at least some Mn^{IV} in the products. The excess of pivalic acid is to prevent formation of insoluble Mn oxides.

The comproportionation reaction of $Mn(O_2CBu^t)_2$, $Mn(ClO_4)_2$, NBu^n_4Cl, and $NBu^n_4MnO_4$ (1:1:1:1) in the presence of pivalic acid in hot MeCN gave a dark brown solution that

Table 2. Selected Bond Distances (Å) and Angles (deg) for 1·3MeCN

parameters		parameters	
Mn1–O3	1.890(3)	Mn4–O3	1.905(3)
Mn1–O1	1.918(3)	Mn4–Cl1	2.7366(16)
Mn1–O12	1.940(3)	Mn5–O2	1.915(3)
Mn1–O11	1.941(3)	Mn5–O1	1.915(3)
Mn1–Cl2	2.4604(15)	Mn5–O4	1.920(3)
Mn1–Cl1	2.7841(16)	Mn5–O6	1.957(3)
Mn2–O1	1.869(3)	Mn6–O4	1.840(3)
Mn2–O2	1.906(3)	Mn6–O6	1.846(3)
Mn2–N3	2.359(17)	Mn6–O5	1.906(3)
Mn2–Cl1	2.6586(15)	Mn7–O7	1.903(3)
Mn3–O3	1.916(3)	Mn7–O6	1.921(3)
Mn3–O4	1.946(3)	Mn7–O5	2.385(4)
Mn3–Cl3	2.2305(14)	Mn8–O2	1.904(3)
Mn3–O5	2.286(3)	Mn8–O7	1.908(4)
Mn3–Cl2	2.5891(14)	Mn8–O9	1.944(4)
Mn4–O7	1.882(3)	Mn8–Cl1	2.8003(15)

Table 3. BVS for the Mn and Selected O Atoms in 1

atom[a]	Mn^{II}	Mn^{III}	Mn^{IV}
Mn1	3.20	**2.99**	3.09
Mn2	3.18	**2.94**	3.07
Mn3	3.10	**2.95**	3.02
Mn4	3.25	**2.99**	3.12
Mn5	3.13	**2.86**	3.00
Mn6	4.24	3.88	**4.07**
Mn7	3.14	**2.87**	3.01
Mn8	3.21	**2.95**	3.08
atom[b]			assgnt
O1	2.03		O^{2-}
O2	1.98		O^{2-}
O3	2.00		O^{2-}
O4	2.04		O^{2-}
O5	1.12		OH^-
O6	2.02		O^{2-}
O7	2.04		O^{2-}
O21	1.02		OH[c]

[a]The bold value is the one closest to the charge for which it was calculated. The Mn oxidation state is the nearest whole number to the bold value. [b]An O BVS of ~1.8–2.0, ~1.0–1.2, and ~0.2–0.4 indicates non-, single-, and double-protonation, respectively, but can be altered somewhat by H-bonding. [c]Pivalic acid.

dx.doi.org/10.1021/ic302021a | Inorg. Chem. 2013, 52, 873–884

Table 4. Known Mn_8 Clusters and Their Metal Oxidation States

complex[a,b]	oxidation state	ref
$[Mn_8O_6(OH)(O_2CBu^t)_9Cl_3(Bu^tCO_2H)_{0.5}(MeCN)_{0.5}]$	Mn^{III}_7, Mn^{IV}	t. w.
$[Mn_8O_9(O_2CBu^t)_{12}]$	Mn^{III}_2, Mn^{IV}_6	t. w.
$[Mn_8(O_2CCH_2Bu^t)_{12}(teaH)_4]$	Mn^{II}_4, Mn^{III}_4,	26
$[Mn_8O_4(piv)_{10}(thme)_2(py)_2]$	Mn^{III}_8	27
$[Mn_8O_{10}(O_2CMe)_6(H_2O)_2(bpy)_6](ClO_4)_4$	Mn^{III}_2, Mn^{IV}_6	28
$(NBu^n_4)[Mn_8O_6C1_6(O_2CPh)_7(H_2O)_2]$	Mn^{III}_8	24a
$[Mn_8O_3(OH)(OMe)(O_2CPh)_7(edte)(edteH_2)](O_2CPh)$	Mn^{II}_2, Mn^{III}_6	29
$[Mn_8(salox)_6O_2(N_3)_6(MeOH)_4]$	Mn^{II}_2, Mn^{III}_6	30
$[Mn_8O_2(OH)_2(OMe)_{12}(OCH_3)_2(Mesalim)_4]$	Mn^{III}_8	31
$(Et_4N)[Mn_8O_4K(pyz)_4(OCH_3)_{14}(CH_3CN)]$	Mn^{III}_8	32
$[Mn(2\text{-mpshz})(dmso)]_8$	Mn^{III}_8	33
$[Mn_8O_4(Me_2Bta)_6(OMe)_2F_8(Me_2BtaH)(MeOH)_8]$	Mn^{III}_8	34
$[Na_2Mn_8O_2(N_3)_8(H_2L)_6Cl]$	Mn^{II}_2, Mn^{III}_6	35
$[Mn_8(DMF)_8(L')_8]$	Mn^{III}_8	36
$[Mn_8O_2(L'')_{12}]$	Mn^{II}_8	37
$[Mn_8O_2(O_2CCH_2Bu^t)_{14}(Bu^tCH_2CO_2H)_4]$	Mn^{II}_6, Mn^{III}_2	38
$[Mn_8O_2(py)_4(O_2CEt)_8(pdm)_2][ClO_4]_2$	Mn^{II}_6, Mn^{III}_2	39
$[Mn_8O_2(OH)_2(O_2CPh)_{10}\{(Ph)(2\text{-py})CNO\}_4]$	Mn^{III}_4, Mn^{II}_4	40
$(NBu^n_4)_2[Mn_8O_4(O_2CPh)_{12}(Et_2mal)_2(H_2O)_2]$	Mn^{II}_2, Mn^{III}_6	41
$[Mn_8O_4(OH)_2(OAc)_{12}(DMHP)_2(py)_2]$	Mn^{II}_2, Mn^{III}_6	42
$[Mn_4O_2(O_2CPh)_6(dbm)_2(bpe)_2]_2$	Mn^{III}_8	43
$[Mn_8O_2(O_2CPh)_{10}(hmp)_4(MeOH)_2]$	Mn^{II}_6, Mn^{III}_2	44
$[Mn_8O_4(phpz)_8(thf)_4]$	Mn^{III}_8	45
$[Mn_8O_2(O_2CEt)_{14}(MeOH)_4]$	Mn^{II}_6, Mn^{III}_2	46
$[Mn_8O_4(OMe)(mpko)_9(mpkoH)](ClO_4)_4$	Mn^{II}_2, Mn^{III}_6	47
$[Mn_8(N_3)_4(O_2CEt)_6(pd)_4(py)_6]$	Mn^{II}_6, Mn^{III}_2	48
$[Mn_8O_4(Hpmide)_4(O_2CEt)_6]$	Mn^{II}_4, Mn^{III}_4	49
$[Mn_8O_2(Naphth\text{-}sao)_6(N_3)_6(MeOH)_8]$	Mn^{II}_2, Mn^{III}_6	50
$[Mn_8O_4(OH)_4(OMe)_2(N_3)_2(dapdo)_2(dapdoH)_2(H_2O)_2]$	Mn^{II}_2, Mn^{III}_6	51
$[Mn_8(O_2CBu^t)_2(tmp)_2(Htmp)_4Br_4(H_2O)_2]$	Mn^{II}_4, Mn^{III}_4	52
$[Mn_8O_4(fdc)_6(DMF)_2(H_2O)_2]$	Mn^{II}_4, Mn^{III}_4	53
$[Mn_8Cl_8(OCH_2CH_2OMe)_4(HOCH_2CH_2OMe)_3]$	Mn^{II}_8	54
$[Mn_8O_2\{(py)_2CO_2\}_4\{(py)_2C(OMe)O\}_2(O_2CEt)_6(HCO_2)]$	Mn^{II}_2, Mn^{III}_6	55

[a]Solvent molecules of crystallization are omitted. [b]Abbreviations: t.w. = this work; tea = triethanolamine; thme = 1,1,1-tris(hydroxymethyl) ethane; bpy = bipyridine; edte = *N*,*N*,*N*′,*N*′-tetrakis(2-hydroxyethyl)ethylenediamine; salox = salicylaldoxime; Mesalim = methyl salicylimidate; pyz = pyrazinate; 2-mpshz = *N*-(2-methyl(propanoyl)salicylhydrazide; Me_2BtaH = dimethylbenzotriazole; H_2L = quinquedentate Schiff base; L′ = *N*-acyl-salicylhydrazides; L″ = 2-amino-3-bromo-5-methylpyridine; pdm = pyridine-2,6-dimethanol; ((Ph)(2-py)CNO) = phenyl 2-pyridyl ketoxime; Et_2mal =2,2-diethylmalonate; DMHP = 2,4-dimethyl-6-hydroxypyrimidine; dbm = dibenzoylmethane; bpe = *trans*-1,2-bis(4-pyridyl)ethane; hmp = 2-hydroxymethylpyridine; phpz = 3-methyl-5-(2-hydroxyphenyl)pyrazole; mpko = methyl 2-pyridyl ketone oxime; pdH_2 = 1,3-propanediol; H_2pmide = *N*-(2-pyridylmethyl)iminodiethanol; $dapdoH_2$ = 2,6-diacetylpyridine dioxime; $tmpH_2$ = 1,1,1-tris(hydroxymethyl)propane, $fdcH_2$ = ferrocene-1,1′-dicarboxylic acid.

subsequently led to isolation of $[Mn_8O_6(OH)(O_2CBu^t)_9Cl_3(Bu^tCO_2H)_{0.5}(MeCN)_{0.5}]$ (**1**; $7Mn^{III}$, Mn^{IV}) in 25% yield. The average Mn oxidation state in the reaction is +4.5, but in the isolated product it is only +3.1. Given the low yield of **1**, it was considered possible that there are higher oxidation state products in the filtrate, but we were unable to isolate any additional compounds to explore this. The use of $Mn(NO_3)_2$ or $MnCl_2$ in place of $Mn(ClO_4)_2$ also led to the isolation of **1**, but in much lower yield.

It was also considered possible that the low content of Mn^{IV} in **1** was due to the highly reactive MnO_4^- oxidizing not just Mn^{II} but also organic groups as it dissipated its oxidizing power. Thus, we also explored the use of an even lower Mn^{II}:Mn^{VII} ratio of 2:3 to increase the average Mn oxidation state to +5 (eq 3).

$$2Mn^{2+} + 3Mn^{7+} \rightarrow 5Mn^{5+} \quad (3)$$

In the procedure to **1**, this unfortunately gave mixtures of products (as evident from two kind of crystals with different unit cell parameters) that we could not separate. However, a simplified procedure comprising $Mn(NO_3)_2$ and $NBu^n_4MnO_4$ (2:3) in the presence of pivalic acid in hot MeCN gave $[Mn_8O_9(O_2CBu^t)_{12}]$ (**2**; $2Mn^{III}$, $6Mn^{IV}$) in 36% isolated yield. The average Mn oxidation state in the product is now +3.75. Interestingly, when $PhCO_2H$ or $EtCO_2H$ were employed instead of Bu^tCO_2H in the procedure to **2**, the products were $[Mn_{12}O_{12}(O_2CR)_{16}(H_2O)_4]$ (R = Ph, Et) with average Mn oxidation state +3.33, emphasizing the importance of the pivalate group (bulk, basicity, etc) in determining the identity of product **2**.

Finally, the procedure to **1** was further investigated by excluding the $Mn(ClO_4)_2$ and NBu^n_4Cl and varying the solvent. The reaction of $Mn(O_2CBu^t)_2$ and $NBu^n_4MnO_4$ in a 1:1 ratio with an excess of pivalic acid in hot MeCN/THF (2:1) led to the isolation of $[Mn_9O_7(O_2CBu^t)_{13}(THF)_2]$ (**3**) in 35% yield. Unlike **1** and **2**, complex **3** is not mixed-valent, containing only Mn^{III} atoms. Clearly, these comproportionation reactions are very complicated and therefore sensitive to many reaction

dx.doi.org/10.1021/ic302021a | *Inorg. Chem.* 2013, 52, 873−884

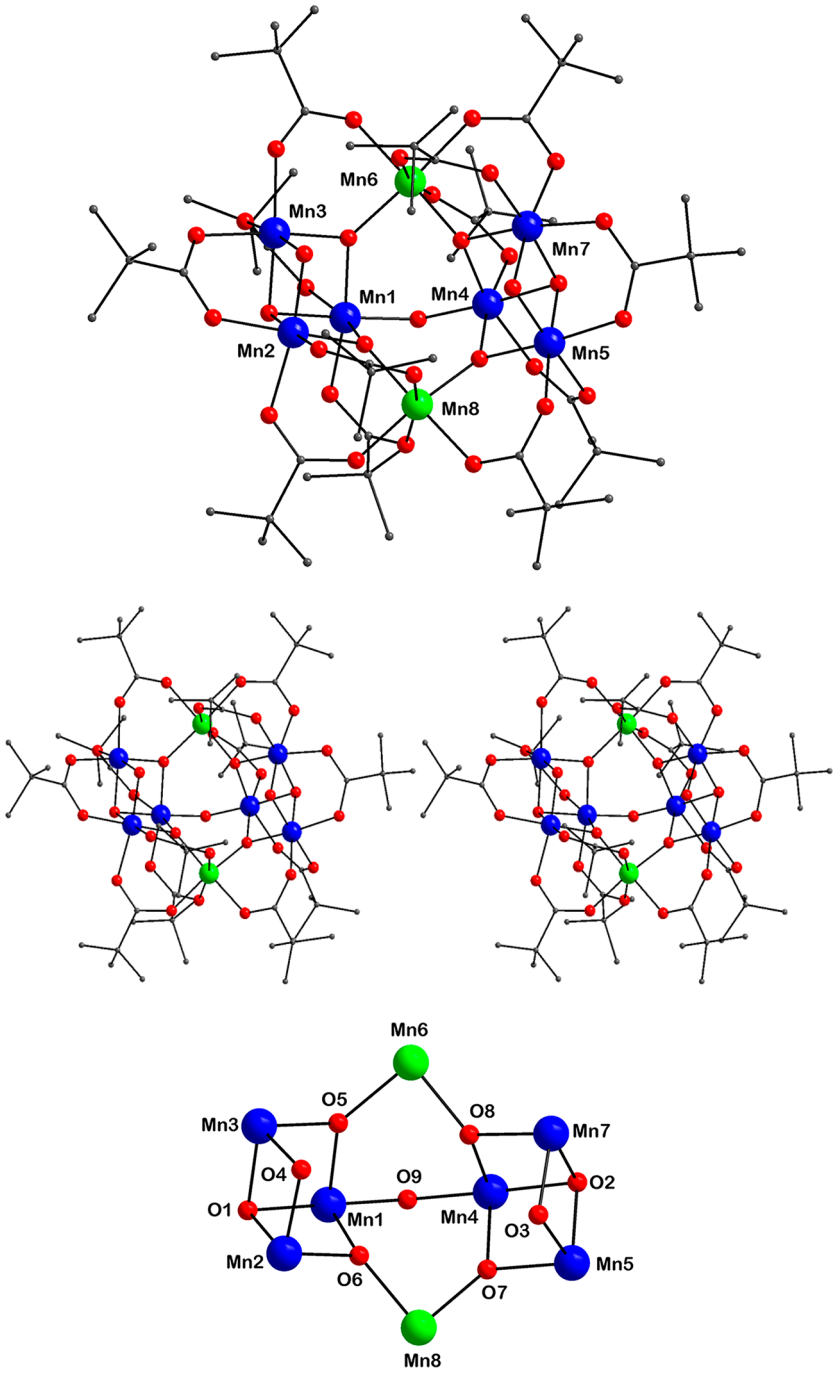

Figure 2. Structure of complex **2** (top), a stereopair (middle), and the labeled core emphasizing the two open faced cubane units (bottom). H atoms have been omitted for clarity. Color code: Mn^{IV} blue; Mn^{III} green; O red; Cl purple; C gray.

parameters, as indeed is the hallmark of higher oxidation state Mn chemistry.

Description of Structures. The structure of **1** is shown in Figure 1, and selected interatomic distances and angles are listed in Table 2. The complex contains a $[Mn_8(\mu_3\text{-}O)_4(\mu_4\text{-}O)_2(\mu_3\text{-}OH)(\mu_4\text{-}Cl)(\mu_2\text{-}Cl)]^{10+}$ core that is mixed valent, $Mn^{III}_7Mn^{IV}$, with Mn6 being the Mn^{IV} atom. The Mn oxidation states and the protonation levels of O^{2-}, OH^-, and carboxylate O atoms were confirmed by bond valence sum (BVS) calculations (Table 3).[23] The core can be described as comprising two $[Mn_4(\mu_3\text{-}O)_2]$ butterfly units, Mn1/Mn2/Mn5/Mn8, and Mn3/Mn5/Mn6/Mn7, fused together by sharing "body" Mn atom Mn5, and giving a near-linear Mn2−Mn5−Mn6 angle (176.5(4)°). The remaining Mn atom, Mn4, is connected to the four "wing-tip" atoms (Mn1/Mn3/Mn7/Mn8) via two $\mu_4\text{-}O^{2-}$ ions O3 and O7, and these become μ_4 by also bridging to Mn5. This makes Mn5 formally seven-coordinate, but in fact the Mn5−O3 and Mn5−O7 bonds are long (2.604(3) and 2.745(3) Å, respectively) and are thus only weak contacts. Finally, there are three additional monatomic bridges: at one end of the core, a $\mu_3\text{-}OH^-$ ion (O5) bridges Mn3/Mn6/Mn7; at the other end, a Cl^- ion (Cl1) bridges the analogous three atoms Mn1/Mn2/Mn8, but also connects to Mn4 to become μ_4; and a $\mu_2\text{-}Cl^-$ (Cl2) bridges Mn1/Mn2. All the Mn centers are six-coordinate, with near-octahedral geometry, except for the ostensibly seven-coordinate

dx.doi.org/10.1021/ic302021a | Inorg. Chem. 2013, 52, 873−884

Table 5. Selected Bond Distances (Å) for Complex 2·MeCN

Mn1−O9	1.7681(14)	Mn4−O8	1.8893(14)
Mn1−O5	1.8794(14)	Mn4−O2	1.9520(16)
Mn1−O6	1.8844(15)	Mn5−O3	1.8057(15)
Mn1−O1	1.9518(14)	Mn5−O7	1.8463(15)
Mn2−O4	1.8149(14)	Mn5−O2	1.8524(14)
Mn2−O1	1.8744(15)	Mn6−O8	1.8583(15)
Mn2−O6	1.8774(14)	Mn6−O5	1.9073(14)
Mn3−O4	1.8058(15)	Mn7−O3	1.8149(14)
Mn3−O5	1.8401(14)	Mn7−O2	1.8733(14)
Mn3−O1	1.8625(14)	Mn8−O6	1.8721(15)
Mn4−O9	1.7642(15)	Mn8−O7	1.8760(13)
Mn4−O7	1.8817(14)		

Table 6. BVS for the Mn Atoms[a] in 2

atom	Mn(II)	Mn(III)	Mn(IV)
Mn1	4.31	3.94	**4.14**
Mn2	4.20	3.84	**4.03**
Mn3	4.25	3.90	**4.08**
Mn4	4.29	3.92	**4.11**
Mn5	4.35	3.98	**4.18**
Mn6	3.31	**3.03**	3.18
Mn7	4.20	3.84	**4.03**
Mn8	3.32	**3.04**	3.19

[a]See footnote *a* of Table 3.

Mn5. The near-octahedral Mn^{III} atoms display the expected Jahn−Teller (JT) axial elongation, the JT axes lying on the Mn−Cl, Mn−OH, and Mn−O (pivalate) bonds, and thus avoiding the Mn−O^{2-} bonds.

The core of **1** is thus surprisingly asymmetric in (i) the location of its Mn^{IV} ion; (ii) the μ_3-OH^- vs μ_4-Cl^- bridges at the two ends; and (iii) a μ-Cl^- ion on only one side of the molecule. In fact, OH^- bridging to a Mn^{IV} is itself rather unusual,[24] as are pyramidal μ_4-Cl^- ions.[25] The asymmetry extends to the peripheral ligation, which consists of nine η^1:η^1:μ-pivalates, one terminal Cl^- on Mn3, and a terminal pivalic acid on Mn2; the latter is disordered with a terminal MeCN ligand on Mn2.

There are quite a few Mn_8 clusters reported in the literature, possessing a wide variety of metal topologies ranging from rodlike, serpentine, rectangular, linked Mn_4 butterfly units, linked tetrahedra, rings, and so forth (Table 4). Only one of these, the $[Mn^{III}{}_8O_6Cl_6(O_2CPh)_7(H_2O)_2]^-$ anion, is related to **1** in containing a similar fused-butterfly unit, but it is homovalent and its core is much more symmetric.[24a] In fact, the $Mn_7{}^{III}Mn^{IV}$ level of **1** is unique for Mn_8 complexes, the others all being $Mn_8{}^{II}$, $Mn_6{}^{II}Mn_2{}^{III}$, $Mn_4{}^{II}Mn_4{}^{III}$, $Mn_2{}^{II}Mn_6{}^{III}$, $Mn_8{}^{III}$ or $Mn_2{}^{III}Mn_6{}^{IV}$ (Table 4).

The structure of $[Mn_8O_9(O_2CBu^t)_{12}]$ (**2**) is shown in Figure 2, and selected interatomic distances and angles are listed in Table 5. The complex contains a $[Mn_8(\mu_3\text{-}O)_6(\mu\text{-}O)_3]^{12+}$ core that, like that in **1**, is mixed-valent, but now at the $Mn^{III}{}_2Mn^{IV}{}_6$ level (Table 6). The core consists of two $Mn^{IV}{}_3O_4$ partial cubane units bridged by μ-O^{2-} ion O9 and the two Mn^{III} atoms Mn6 and Mn8. All Mn atoms are near-octahedral, and the Mn^{III} JT elongation axes involve only carboxylate groups (O23−Mn6−O28 and O32−Mn8−O10) and are nearly parallel. The peripheral ligation is by twelve η^1:η^1:μ-pivalate groups. The molecule has virtual C_2 symmetry with the C_2 rotation axis passing through the μ-O^{2-} ion O9. The core is without precedent among known Mn_8 clusters, and is only the second example at the $Mn_2{}^{III}Mn_6{}^{IV}$ oxidation level.[27]

The structure of $[Mn_9O_7(O_2CBu^t)_{13}(THF)_2]$ (**3**) is shown in Figure 3, and selected interatomic distances and angles are listed in Table 7. The complex contains a $[Mn_9{}^{III}(\mu_3\text{-}O)_7]^{13+}$ core and is unlike **1** and **2** in being homovalent, that is, $9Mn^{III}$ (Table 8). Like **1**, complex **2** contains two Mn_4 butterfly units, Mn9/Mn3/Mn2/Mn6 and Mn8/Mn2/Mn1/Mn5, fused at body atom Mn2. This unit is connected to two Mn atoms, Mn4 and Mn7, by three additional μ_3-O^{2-} ions, O8/O18/O29. As a result, the Mn1−Mn2−Mn3 angle deviates markedly from linearity (143°). All the Mn^{III} are near-octahedral and display JT elongations. The peripheral ligation is by eleven η^1:η^1:μ-pivalate groups, two pivalates in the rarer η^1:η^2:μ mode, and two terminal THF groups. Although complex **3** has not been made before, its Mn_9 core is very similar to those in some previous complexes.[24a,S6,S7]

Magnetochemistry. Solid-state, variable-temperature dc magnetic susceptibility data in the 5.0−300.0 K range in a 0.1 T field were collected on powdered microcrystalline samples of **1**·MeCN, **2**·$^1/_4$MeCN, and **3** restrained in eicosane to prevent torquing. The obtained data are plotted as $\chi_M T$ vs T in Figure 4. $\chi_M T$ for **1**·MeCN is 22.0 cm^3 K mol^{-1} at 300 K, comparable with the 22.88 cm^3 K mol^{-1} for seven Mn^{III} and one Mn^{IV} noninteracting atoms with g = 2. It slowly increases with decreasing temperature to a maximum of 27.27 cm^3 K mol^{-1} at 15 K, and then slightly drops to 26.06 cm^3 K mol^{-1} at 5.0 K. This profile indicates that at least some interactions are ferromagnetic, and that the molecule has a large ground state spin, S. $\chi_M T$ at the lowest temperatures suggests an $S = {}^{15}/_2$ ground state (spin-only value is 31.88 cm^3 K mol^{-1}) with g slightly <2, as expected for a Mn^{III}/Mn^{IV} complex. The $\chi_M T$ for **2**·$^1/_4$MeCN is 13.75 cm^3 K mol^{-1} at 300 K, lower than the 17.25 cm^3 K mol^{-1} expected for six Mn^{IV} and two Mn^{III} noninteracting atoms with g = 2.0, and it decreases steadily with decreasing temperature to 3.55 cm^3 K mol^{-1} at 5.0 K. This indicates the presence of dominant antiferromagnetic interactions, and the 5.0 K value suggests an S = 1 or 2 ground state. Similarly, $\chi_M T$ for **3** is 19.81 cm^3 K mol^{-1} at 300 K, lower than the spin-only value of 27.00 cm^3 K mol^{-1} expected for nine noninteracting Mn^{III} atoms, and it decreases steadily with decreasing temperature to 2.70 cm^3 K mol^{-1} at 5.0 K. This again indicates the presence of dominant antiferromagnetic interactions, and the 5.0 K value indicates a low ground state spin of S = 0 or 1.

To probe the ground states of **1**−**3** further, and to determine the zero-field splitting parameter (D), magnetization (M) vs field (H) data were collected in the magnetic field and temperature ranges of 0.1−7 T and 1.8−10 K, respectively. The resulting data for **1**·MeCN are plotted in Figure 5 as reduced magnetization ($M/N\mu_B$) vs H/T, where N is Avogadro's number and μ_B is the Bohr magneton. The data were fit by diagonalization of the spin Hamiltonian matrix, using the program MAGNET, which assumes only the ground state is populated, includes the Zeeman interaction and axial zero-field splitting ($D\hat{S}_z{}^2$), and incorporates a full powder average. The corresponding spin Hamiltonian is given by eq 4,

$$H = D\hat{S}_z{}^2 + g\mu_B\mu_0\hat{S}\cdot H \quad (4)$$

where $\hat{S}_z$ is the easy-axis spin operator, and μ_0 is the vacuum permeability. The last term is the Zeeman energy associated with the applied magnetic field. A satisfactory fit could only be

dx.doi.org/10.1021/ic302021a | Inorg. Chem. 2013, 52, 873−884

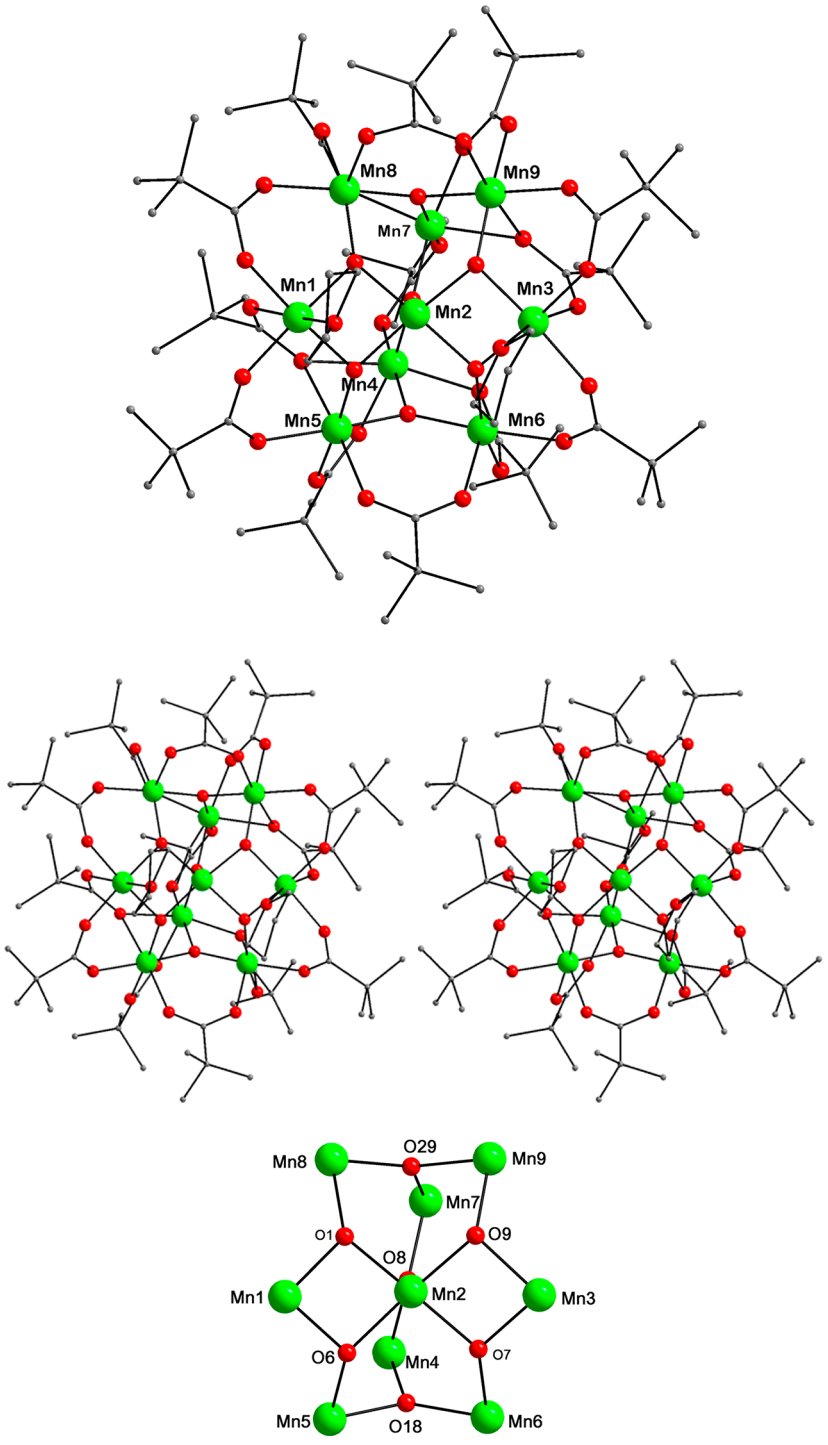

Figure 3. Structure of complex **3** (top), a stereopair (middle), and the labeled core (bottom). H atoms have been omitted for clarity. Color code: Mn^{III} green; O red; C gray.

obtained if data collected at fields above 4 T were excluded, suggesting that some low-lying excited states with greater spin than the ground state are being stabilized by the applied field and causing them to be significantly populated. The obtained fit (solid lines in Figure 5) gave $S = {}^{15}/_{2}$, $g = 1.98(2)$ and $D = -0.22(2)$ cm^{-1}. Alternative fits with $S = {}^{17}/_{2}$, $g = 1.65(2)$, $D = -0.22(2)$ cm^{-1} and $S = {}^{13}/_{2}$, $g = 2.14(2)$, $D = -0.37(2)$ cm^{-1} were rejected because of their unreasonable g values. The best fit with all data up to 7 T is shown in Supporting Information, Figure S1.

For **2**·${}^{1}/_{4}$MeCN and **3**, no satisfactory fits could be obtained even using just low-field data, suggesting particularly low-lying excited states in these complexes (Supporting Information, Figures S2 and S3). This is a common problem in higher nuclearity clusters and/or ones containing extensive spin frustration effects arising from the presence of many triangular units involving competing exchange interactions. Fortunately, **1**·MeCN did not suffer problems from very low-lying excited states, even though it is also high nuclearity and contains triangular units.

dx.doi.org/10.1021/ic302021a | *Inorg. Chem.* 2013, 52, 873−884

Table 7. Selected Bond Distances (Å) for $3\cdot{}^{1}/_{3}$THF$\cdot{}^{2}/_{3}$MeCN

Mn1–O1	1.865(2)	Mn5–O6	1.871(2)
Mn1–O6	1.866(2)	Mn5–O18	1.880(2)
Mn2–O7	1.898(2)	Mn6–O18	1.858(2)
Mn2–O1	1.902(2)	Mn6–O7	1.874(2)
Mn2–O9	1.926(2)	Mn7–O8	1.857(2)
Mn2–O6	1.938(2)	Mn7–O29	1.881(2)
Mn2–O8	2.178(2)	Mn8–O29	1.864(2)
Mn3–O7	1.861(2)	Mn8–O1	1.873(2)
Mn3–O9	1.871(2)	Mn9–O29	1.882(2)
Mn4–O8	1.861(2)	Mn9–O9	1.883(2)
Mn4–O18	1.886(2)		

Table 8. BVS for the Mn Atoms[a] in 3

atom	Mn(II)	Mn(III)	Mn(IV)
Mn1	3.29	**3.02**	3.17
Mn2	2.99	**2.73**	2.87
Mn3	3.27	**2.99**	3.14
Mn4	3.59	**2.89**	3.48
Mn5	3.29	**3.01**	3.16
Mn6	3.20	**2.93**	3.08
Mn7	3.28	**2.91**	3.05
Mn8	3.18	**2.91**	3.05
Mn9	3.24	**2.97**	3.11

[a]See footnote *a* of Table 3.

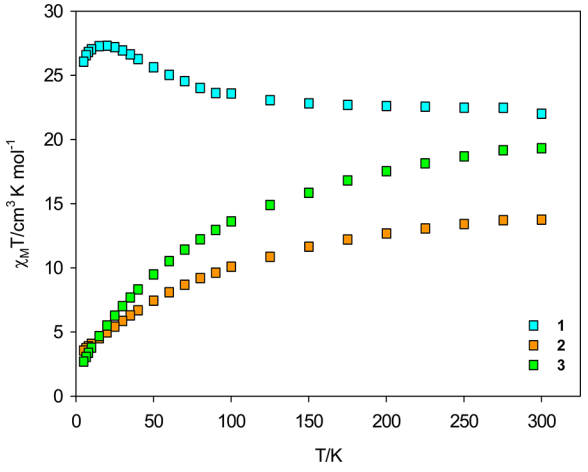

Figure 4. Plot of $\chi_M T$ vs T for complexes **1**·MeCN, $\mathbf{2}\cdot{}^{1}/_{4}$MeCN, and **3**.

AC Susceptibility Studies. These were carried out to determine or confirm the ground states, and also to probe the magnetization relaxation dynamics. They were performed using a 3.5 G ac field oscillating at frequencies in the 50–1000 Hz. For **1**·MeCN, there is a near-plateau in the in-phase $\chi'_M T$ vs T plot above ~6 K of ~28.5 cm^3 K mol^{-1} (Figure 6) consistent with an $S = {}^{15}/_{2}$ ground state and $g < 2$, in agreement with the dc data. At lower temperatures, there is a slight decrease assignable to ZFS and weak intermolecular interactions, and below 3 K there is a greater decrease in $\chi'_M T$ and the concomitant appearance of an out-of-phase χ''_M signal. Both of these are frequency-dependent, suggesting the slow relaxation of a SMM. Confirmation of this required magnetization hysteresis studies, and these are described below.

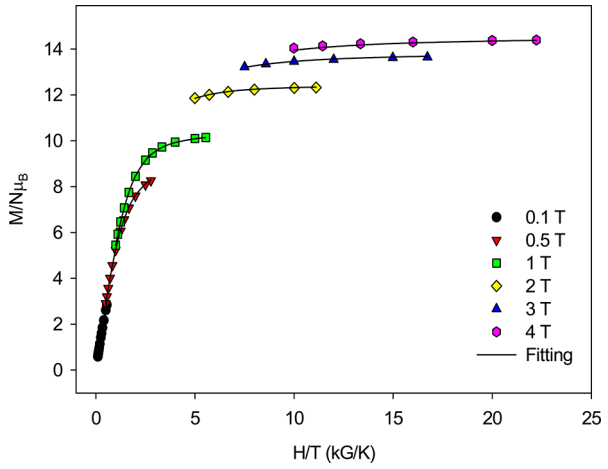

Figure 5. Plot of reduced magnetization ($M/N\mu_B$) vs H/T for complex **1**·MeCN. The solid lines are the fit of the data; see the text for the fit parameters.

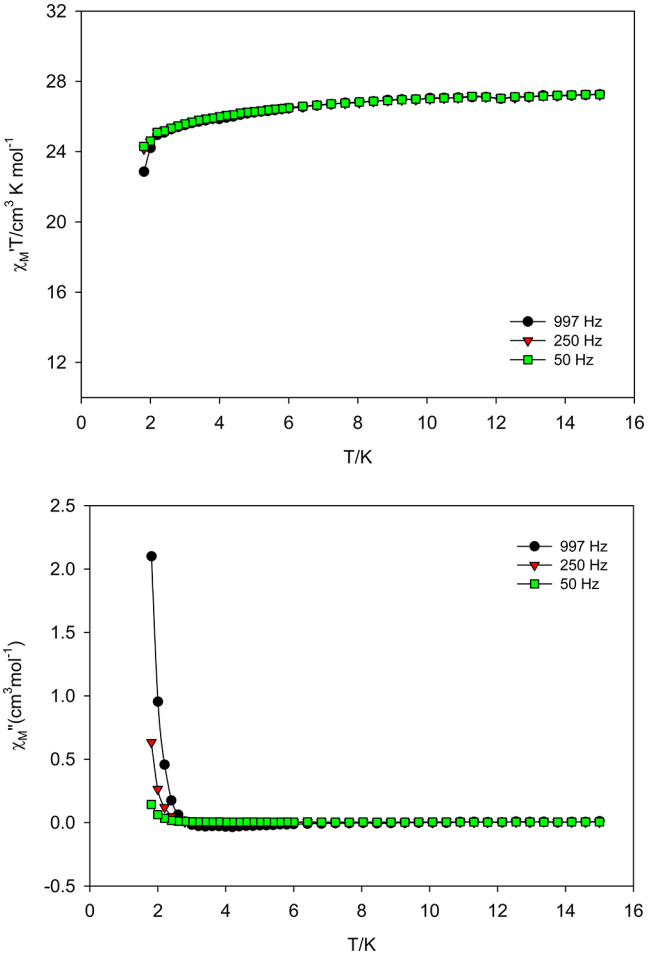

Figure 6. AC susceptibility of complex **1**·MeCN in a 3.5 G field oscillating at the indicated frequencies: (top) in-phase signal (χ'_M) plotted as $\chi'_M T$ vs T; and (bottom) out-of-phase signal (χ''_M) vs T.

The in-phase $\chi'_M T$ vs T plot for $\mathbf{2}\cdot{}^{1}/_{4}$MeCN (Figure 7, top) shows a steady decrease in $\chi'_M T$ value with decrease in temperature, consistent with depopulation of one or more low-lying excited states with S greater than the ground state; this rationalizes the bad fit of magnetization vs dc field data described above. Extrapolation of the plot from above 3 K (to

dx.doi.org/10.1021/ic302021a | Inorg. Chem. 2013, 52, 873–884

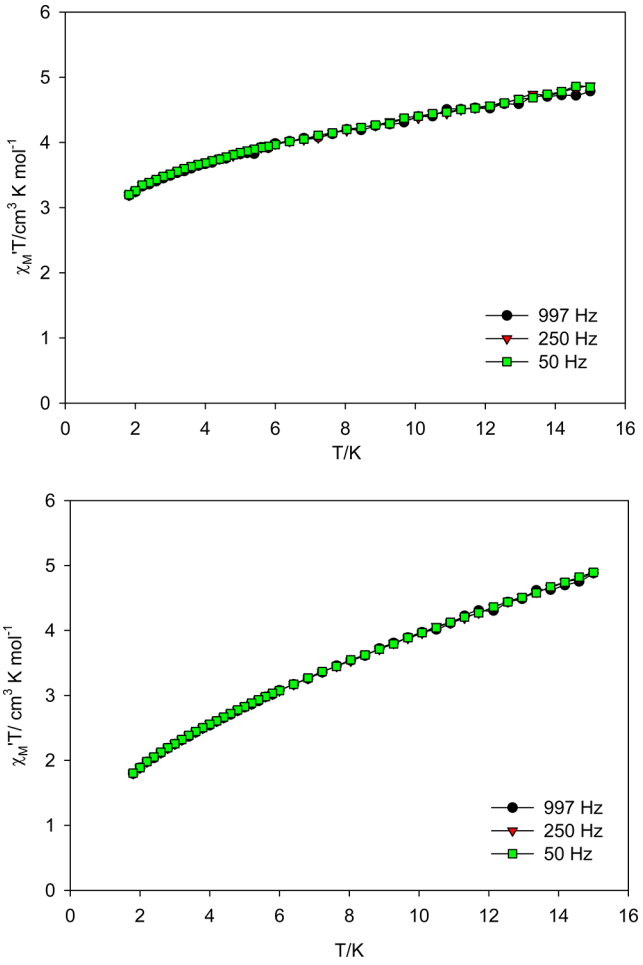

Figure 7. In-phase AC magnetic susceptibility of complex $2\cdot{}^1/_4$MeCN (top) and complex **3** (bottom) in a 3.5 G field oscillating at the indicated frequencies plotted as $\chi'_M T$ vs T.

avoid the effect of weak intermolecular interactions) to 0 K gives a $\chi'_M T$ of ~3.0 cm^3 K mol^{-1} indicating an $S = 2$ ground state with $g \sim 2$; $S = 1$ and $S = 3$ would give $\chi'_M T$ of ~1.0 and ~6.0 cm^3 K mol^{-1}, respectively, which clearly differ from the experimental data. We thus feel confident in a conclusion that $2\cdot{}^1/_4$MeCN has an $S = 2$ ground state.

The $\chi'_M T$ vs T for **3** (Figure 7, bottom) shows a similar profile to that of $2\cdot{}^1/_4$MeCN, but is even more steeply decreasing with decreasing T, suggesting a higher density of low-lying excited states. This makes an extrapolation more unreliable, but the plot is heading for the $\chi'_M T$ ~1.0 K region indicating an $S = 1$ ground state; $S = 0$ and $S = 2$ would give $\chi'_M T$ of 0.0 and ~3.0 cm^3 K mol^{-1}, respectively. Neither $2\cdot{}^1/_4$MeCN nor **3** exhibited out-of-phase χ''_M signals above 1.8 K.

Single-Crystal Hysteresis Studies. To confirm whether **1** is an SMM, magnetization vs dc field scans were carried out using a micro-SQUID apparatus on a single crystal of **1**·3MeCN that had been maintained wet with mother liquor. Hysteresis loops were indeed observed, whose coercivities increase with decreasing temperature (Figure 8, top) and increasing scan rate (Figure 8, bottom), as expected for an SMM below its blocking temperature (T_B). These loops thus confirm **1**·3MeCN to be a new addition to the family of SMMs with a half-integer spin.

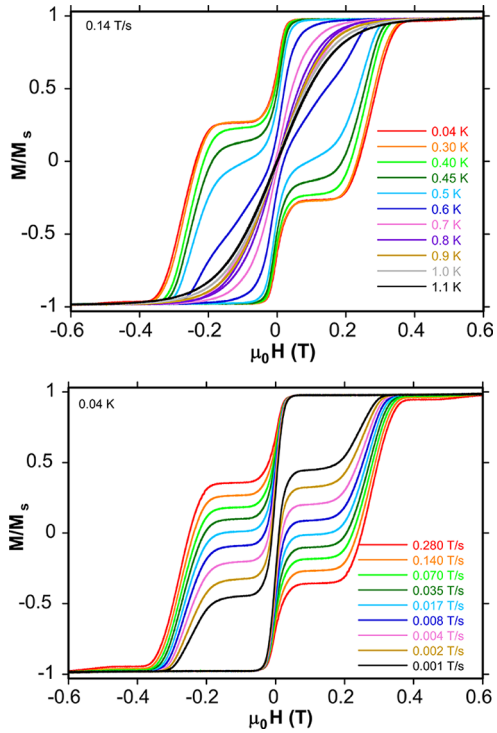

Figure 8. Magnetization (M) vs dc field hysteresis loops for a single crystal of **1**·3MeCN at (top) the indicated field sweep rates and a fixed temperature of 0.04 K, and (bottom) at the indicated temperatures and a fixed field sweep rate of 0.14 T/s. The magnetization is normalized to its saturation value, M_s.

The loops display two well-resolved quantum tunneling of magnetization (QTM) steps. Complex **1** is a half-integer species that should not show QTM in the absence of transverse fields, but these are provided by the transverse components of dipolar and exchange fields from neighboring molecules, and hyperfine fields from ^{55}Mn ($I = {}^5/_2$, 100%) nuclei.[9,58] The first step at zero field is quite sharp (narrow) while the second at ±0.28(1) T is unusually broad, with a total width of almost 0.2 T. We assign this as reflecting the range of molecular environments in the crystal due to the extensive ligand disorder observed in the crystal structure, particularly the rotational disorder of five pivalates, and the pivalic acid vs MeCN disorder at one of the terminal ligands, as well as the disordered solvent molecules. A range of environments means a range of properties, including the D value. Since the latter determines the separation between QTM steps (because it determines the separation between M_S levels), a range of D will give broadened steps at nonzero fields. In contrast, the zero-field step position is not so affected by a range of D values. Weak intermolecular interactions will also contribute to broadening effects. The average D value can be estimated from the step separation (ΔH) of 0.28(1) T using eq 5, which gives

$$\Delta H = |D|/g\mu_B \quad (5)$$

$|D|/g = 0.13(1)$ cm^{-1} ($|D| \approx 0.26$ cm^{-1} for $g = 2$). This is in acceptable agreement with the fit of magnetization data in Figure 5, whose $D = -0.22(2)$ cm^{-1} and $g = 1.98(2)$ values give $|D|/g = 0.11(1)$ cm^{-1}. At temperatures of ~0.3 K and below, the hysteresis loops become essentially temperature-independent, indicating that all tunneling through the anisotropy barrier is now via the ground state $M_s = \pm{}^{15}/_2$ levels of the $S = {}^{15}/_2$ manifold. The relaxation rate at zero applied field is relatively

dx.doi.org/10.1021/ic302021a | Inorg. Chem. 2013, 52, 873−884

fast at most temperatures, as reflected in the large size of the step at this position, and this prevented construction of an Arrhenius plot to determine the magnitude of the effective anisotropy barrier, U_{eff}. The fast relaxation is also evident in the magnetization vs time decay plots of Supporting Information, Figure S4; this figure also more clearly reveals that the temperature-independent relaxation regime is 0.25 K and below.

CONCLUSIONS

The use of a comproportionation reaction between Mn^{II} and Mn^{VII} in the presence of an excess of pivalic acid has proven to be a successful route to new octanuclear manganese(III/IV) clusters, as well as a new derivative of a known class of Mn^{III}_9 clusters. The two Mn_8 products possess unprecedented core topologies and Mn manganese oxidation levels, namely, $Mn^{III}_7Mn^{IV}$ (**1**) and $Mn^{III}_2Mn^{IV}_6$ (**2**). In fact, **2** is only the second homometallic Mn cluster to possess such a high average manganese oxidation state of +3.67. Thus, although Mn/O/pivalate chemistry is with precedent in the literature, the present routes have allowed access into some mixed-valent $Mn^{III/IV}$ structural types not seen before with pivalate or any carboxylate. As a result, this work has also yielded a new half-integer SMM with an $S = {}^{15}/_{2}$ ground state and which displays well resolved QTM steps. Further work in this area is in progress.

ASSOCIATED CONTENT

Supporting Information

X-ray crystallographic files in CIF format for complex **1**·3MeCN, **2**·MeCN, and **3**·${}^{1}/_{3}$THF·${}^{2}/_{3}$MeCN; oxygen bond valence sums for **2** and **3**; and additional magnetic data for **1**·MeCN, **2**·${}^{1}/_{4}$MeCN, **3**, and **1**·3MeCN. This material is available free of charge via the Internet at http://pubs.acs.org.

AUTHOR INFORMATION

Corresponding Author

*Phone: +1-352-392-8314. Fax: +1-352-392-8757. E-mail: christou@chem.ufl.edu.

Notes

The authors declare no competing financial interest.

ACKNOWLEDGMENTS

We thank the National Science Foundation (CHE-0910472) and the ERC Advanced Grant MolNanoSpin No. 226558 for support of this work.

REFERENCES

(1) (a) Law, N. A.; Caudle, M. T.; Pecoraro, V. L. *Adv. Inorg. Chem.* **1999**, *46*, 305. (b) Barber, J. *Chem. Soc. Rev.* **2009**, *38*, 185. (c) Ferreira, K. N.; Iverson, T. M.; Maghlaoui, K.; Barber, J.; Iwata, S. *Science* **2004**, *303*, 1831. (d) Umena, Y.; Kawakami, K.; Shen, J. R.; Kamiya, N. *Nature* **2011**, *473*, 55.

(2) (a) Mukherjee, S.; Stull, J. A.; Yano, J.; Stamatatos, T. C.; Pringouri, K.; Stich, T. A.; Abboud, K. A.; Britt, R. D.; Yachandra, V. K.; Christou, G. *Proc. Natl. Acad. Sci. U.S.A.* **2012**, *109*, 2257. (b) Kanady, J. S.; Tsui, E. Y.; Day, M. W.; Agapie, T. *Science* **2011**, *333*, 733.

(3) Arndt, D. *Manganese Compounds as Oxidizing Agents in Organic Chemistry*; Open Court Publishing Company: Chicago, IL, 1981.

(4) Larsen, A. S.; Wang, K.; Lockwood, M. A.; Rice, G. L.; Won, T. J.; Lovell, S.; Sadilek, M.; Turecek, F.; Mayer, J. M. *J. Am. Chem. Soc.* **2002**, *124*, 10112.

(5) Kahn, O. *Chem. Phys. Lett.* **1997**, *265*, 109.

(6) (a) Christou, G.; Gatteschi, D.; Hendrickson, D. N.; Sessoli, R. *MRS Bull.* **2000**, *25*, 66. (b) Gatteschi, D.; Sessoli, R. *Angew. Chem., Int. Ed.* **2003**, *42*, 268. (c) Christou, G. *Polyhedron* **2005**, *24*, 2065. (d) Aromi, G.; Brechin, E. K. *Struct. Bonding (Berlin)* **2006**, *122*, 1. (e) Bagai, R.; Christou, G. *Chem. Soc. Rev.* **2009**, *38*, 1011.

(7) (a) Bircher, R.; Chaboussant, G.; Dobe, C.; Gudel, H. U.; Ochsenbein, S. T.; Sieber, A.; Waldmann, O. *Adv. Funct. Mater.* **2006**, *16*, 209. (b) Aubin, S. M. J.; Dilley, N. R.; Wemple, M. W.; Maple, N. B.; Christou, G.; Hendrickson, D. N. *J. Am. Chem. Soc.* **1998**, *120*, 839. (c) Kostakis, G. E.; Ako, A. M.; Powell, A. K. *Chem. Soc. Rev.* **2010**, *39*, 2238. (d) Tasiopoulos, A. J.; Perlepes, S. P. *Dalton Trans.* **2008**, 5537. (e) Brechin, E. K. *Chem. Commun.* **2005**, 5141. (f) Aromi, G.; Aubin, S. M. J.; Bolcar, M. A.; Christou, G.; Eppley, H. J.; Folting, K.; Hendrickson, D. N.; Huffman, J. C.; Squire, R. C.; Tsai, H. L.; Wang, S.; Wemple, M. W. *Polyhedron* **1998**, *17*, 3005.

(8) (a) Thomas, L.; Lionti, F.; Ballou, R.; Gatteschi, D.; Sessoli, R.; Barbara, B. *Nature* **1996**, *383*, 145. (b) del Barco, E.; Kent, A. D.; Hill, S.; North, J. M.; Dalal, N. S.; Rumberger, E. M.; Hendrickson, D. N.; Chakov, N.; Christou, G. *J. Low Temp. Phys.* **2005**, *140*, 119.

(9) (a) Wernsdorfer, W.; Sessoli, R. *Science* **1999**, *284*, 133. (b) Wernsdorfer, W.; Soler, M.; Christou, G.; Hendrickson, D. N. *J. Appl. Phys.* **2002**, *91*, 7164. (c) Wernsdorfer, W.; Chakov, N. E.; Christou, G. *Phys. Rev. Lett.* **2005**, 95.

(10) Wemple, M. W.; Tsai, H.-L.; Wang, S.; Claude, J.-P.; Streib, W. E.; Huffman, J. C.; Hendrickson, D. N.; Christou, G. *Inorg. Chem.* **1996**, *35*, 6450.

(11) Libby, E.; McCusker, J. K.; Schmitt, E. A.; Folting, K.; Hendrickson, D. N.; Christou, G. *Inorg. Chem.* **1991**, *30*, 3486.

(12) Hessel, L. W.; Romers, C. *Red. Trav. Chim. Pay-Bas* **1969**, *88*, 545.

(13) Lis, T. *Acta. Crystallogr., Sect. B* **1980**, *836*, 2042.

(14) Stamatatos, T. C.; Christou, G. *Philos. Trans. R. Soc.* **2008**, *366*, 113−125.

(15) For example, see Mukhopadhyay, S.; Mandal, S. K.; Bhaduri, S.; Armstrong, W. H. *Chem. Rev.* **2004**, *104*, 3981.

(16) Stamatatos, T. C.; Vinslava, A.; Abboud, K. A.; Christou, G. *Chem. Commun.* **2009**, 2839.

(17) Vincent, J. B.; Folting, K.; Huffman, J. C.; Christou, G. *Inorg. Chem.* **1986**, *25*, 996.

(18) Yu, S. B.; Lippard, S. J.; Shweky, I.; Bino, A. *Inorg. Chem.* **1992**, *31*, 3502.

(19) *SHELXTL6*; Bruker, AXS: Madison, WI, 2000.

(20) Vandersluis, P.; Spek, A. L. *Acta Crystallogr., Sect. A* **1990**, *46*, 194.

(21) Weast, R. C. *CRC Handbook of Chemistry and Physics*; CRC Press, Inc.: Boca Raton, FL, 1984.

(22) Wernsdorfer, W. *Adv. Chem. Phys.* **2001**, *118*, 99.

(23) (a) Liu, W.; Thorp, H. H. *Inorg. Chem.* **1993**, *32*, 4102. (b) Brown, I. D.; Altermatt, D. *Acta. Crystallogr., Sect. B* **1985**, 244.

(24) (a) Hagen, K. S.; Westmoreland, T. D.; Scott, M. J.; Armstrong, W. H. *J. Am. Chem. Soc.* **1989**, *111*, 1907. (b) Niemann, A.; Bossek, U.; Wieghardt, K.; Butzlaff, C.; Trautwein, A. X.; Nuber, B. *Angew. Chem., Int. Ed. Engl.* **1992**, *31*, 311. (c) Dube, C. E.; Wright, D. W.; Armstrong, W. H. *J. Am. Chem. Soc.* **1996**, *118*, 10910. (d) Larson, E. J.; Riggs, P. J.; Penner-Hahn, J. E.; Pecoraro, V. L. *J. Chem. Soc., Chem. Commun.* **1992**, 102. (e) Chen, H.; Collomb, M.-N.; Duboc, C.; Blondin, G.; Rivière, E.; Faller, J. W.; Crabtree, R. H.; Brudvig, G. W. *Inorg. Chem.* **2005**, *44*, 9567.

(25) (a) Tsai, H.-L.; Wang, S.; Folting, K.; Streib, W. E.; Hendrickson, D. N.; Christou, G. *J. Am. Chem. Soc.* **1995**, *117*, 2503. (b) Schugar, H. J.; Ou, C. C.; Thich, J. A.; Potenza, J. A.; Felthouse, T. R.; Haddad, M. S.; Hendrickson, D. N.; Furey, W.; Lalancette, R. A. *Inorg. Chem.* **1980**, *19*, 543. (c) Kiskin, M. A.; Aleksandrov, G. G.; Ikorskii, V. N.; Novotortsev, V. M.; Eremenko, I. L. *Inorg. Chem. Commun.* **2007**, *10*, 997.

(26) Murugesu, M.; Wernsdorfer, F.; Abboud, K. A.; Christou, G. *Angew. Chem., Int. Ed.* **2005**, *44*, 892.

(27) Brechin, E. K.; Soler, M.; Christou, G.; Helliwell, M.; Teat, S. J.; Wernsdorfer, W. *Chem. Commun.* **2003**, 1276.
(28) Tasiopoulos, A. J.; Abboud, K. A.; Christou, G. *Chem. Commun.* **2003**, 580.
(29) Bagai, R.; Abboud, K. A.; Christou, G. *Inorg. Chem.* **2008**, *47*, 621.
(30) Feng, P. L.; Hendrickson, D. N. *Inorg. Chem.* **2010**, *49*, 6393.
(31) Godbole, M. D.; Roubeau, O.; Clerac, R.; Kooijman, H.; Spek, A. L.; Bouwman, E. *Chem. Commun.* **2005**, 3715.
(32) Huang, D.; Zhang, X.; Ma, C.; Chen, H.; Chen, C.; Liu, Q.; Zhang, C.; Liao, D.; Li, L. *Dalton Trans.* **2007**, 680.
(33) John, R. P.; Lee, K.; Kim, B. J.; Suh, B. J.; Rhee, H.; Lah, M. S. *Inorg. Chem.* **2005**, *44*, 7109.
(34) Jones, L. F.; Raftery, J.; Teat, S. J.; Collison, D.; Brechin, E. K. *Polyhedron* **2005**, *24*, 2443.
(35) Liu, D.; Zhou, Q.; Chen, Y.; Yang, F.; Yu, Y.; Shi, Z.; Feng, S. H. *Dalton Trans.* **2010**, *39*, 5504.
(36) Luo, W.; Wang, X. T.; Meng, X. G.; Cheng, G. Z.; Ji, Z. P. *Polyhedron* **2009**, *28*, 300.
(37) Alvareza, C. S.; Bond, A. D.; Cave, D.; Mosquera, M. E. G.; Harron, E. A.; Layfield, R. A.; McPartlin, M.; Rawson, J. M.; Wood, P. T.; Wright, D. S. *Chem. Commun.* **2002**, 2980.
(38) Boskovic, C.; Huffman, J. C.; Christou, G. *Chem. Commun.* **2002**, 2502.
(39) Boskovic, C.; Wernsdorfer, W.; Folting, K.; Huffman, J. C.; Hendrickson, D. N.; Christou, G. *Inorg. Chem.* **2002**, *41*, 5107.
(40) Milios, C. J.; Stamatatos, T. C.; Kyritsis, P.; Terzis, A.; Raptopoulou, C. P.; Vicente, R.; Escuer, A.; Perlepes, S. P. *Eur. J. Inorg. Chem.* **2004**, 2885.
(41) Wemple, M. W.; Tsai, H. L.; Wang, S. Y.; Claude, J. P.; Streib, W. E.; Huffman, J. C.; Hendrickson, D. N.; Christou, G. *Inorg. Chem.* **1996**, *35*, 6437.
(42) Brechin, E. K.; Christou, G.; Soler, M.; Helliwell, M.; Teat, S. J. *Dalton Trans.* **2003**, 513.
(43) Wang, S.; Tsai, H. L.; Folting, K.; Martin, J. D.; Hendrickson, D. N.; Christou, G. *J. Chem. Soc., Chem. Commun.* **1994**, 671.
(44) Taguchi, T.; Wernsdorfer, W.; Abboud, K. A.; Christou, G. *Inorg. Chem.* **2010**, *49*, 10579.
(45) Tanase, S.; Aromi, G.; Bouwman, E.; Kooijman, H.; Spek, A. L.; Reedijk, J. *Chem. Commun.* **2005**, 3147.
(46) Stamatatos, T. C.; Abboud, K. A.; Christou, G. *J. Mol. Struct.* **2008**, *890*, 263.
(47) Stoumpos, C. C.; Stamatatos, T. C.; Sartzi, H.; Roubeau, O.; Tasiopoulos, A. J.; Nastopoulos, V.; Teat, S. J.; Christou, G.; Perlepes, S. P. *Dalton Trans.* **2009**, 1004.
(48) Moushi, E. E.; Stamatatos, T. C.; Nastopoulos, V.; Christou, G.; Tasiopoulos, A. J. *Polyhedron* **2009**, *28*, 3203.
(49) Wu, C. C.; Datta, S.; Wernsdorfer, W.; Lee, G. H.; Hill, S.; Yang, E. C. *Dalton Trans.* **2010**, *39*, 10160.
(50) Milios, C. J.; Inglis, R.; Jones, L. F.; Prescimone, A.; Parsons, S.; Wernsdorfer, W.; Brechin, E. K. *Dalton Trans.* **2009**, 2812.
(51) Stamatatos, T. C.; Luisi, B. S.; Moulton, B.; Christou, G. *Inorg. Chem.* **2008**, *47*, 1134.
(52) Milios, C. J.; Fabbiani, F. P. A.; Parsons, S.; Murugesu, M.; Christou, G.; Brechin, E. K. *Dalton Trans.* **2006**, 351.
(53) Masello, A.; Murugesu, M.; Abboud, K. A.; Christou, G. *Polyhedron* **2007**, *26*, 2276.
(54) Jerzykiewicz, L. B.; Utko, J.; Duczmalb, M.; Sobota, P. *Dalton Trans.* **2007**, 825.
(55) Stoumpos, C. C.; Roubeau, O.; Aromí, G.; Tasiopoulos, A. J.; Nastopoulos, V.; Escuer, A.; Perlepes, S. P. *Inorg. Chem.* **2010**, *49*, 359.
(56) Shanmugam, M.; Chastanet, G.; Mallah, T.; Sessoli, R.; Teat, S. J.; Timco, G. A.; Winpenny, R. E. P. *Chem.—Eur. J.* **2006**, *12*, 8777.
(57) Chakov, N. E.; Zakharov, L. N.; Rheingold, A. L.; Abboud, K. A.; Christou, G. *Inorg. Chem.* **2005**, *44*, 4555.
(58) Wernsdorfer, W.; Bhaduri, S.; Boskovic, C.; Christou, G.; Hendrickson, D. N. *Phys. Rev. B* **2002**, 65.